

Nanomechanics of Extracellular Vesicles Reveals Vesiculation Pathways

Raya Sorkin,* Rick Huisjes, Filip Bošković, Daan Vorselen, Silvia Pignatelli, Yifat Ofir-Birin, Joames K. Freitas Leal, Jürgen Schiller, Debakshi Mullick, Wouter H. Roos, Giel Bosman, Neta Regev-Rudzki, Raymond M. Schiffelers, and Gijs J. L. Wuite*

Extracellular vesicles (EVs) are emerging as important mediators of cell–cell communication as well as potential disease biomarkers and drug delivery vehicles. However, the mechanical properties of these vesicles are largely unknown, and processes leading to microvesicle-shedding from the plasma membrane are not well understood. Here an in depth atomic force microscopy force spectroscopy study of the mechanical properties of natural EVs is presented. It is found that several natural vesicles of different origin have a different composition of lipids and proteins, but similar mechanical properties. However, vesicles generated by red blood cells (RBC) at different temperatures/incubation times are different mechanically. Quantifying the lipid content of EVs reveals that their stiffness decreases with the increase in their protein/lipid ratio. Further, by maintaining RBC at “extreme” nonphysiological conditions, the cells are pushed to utilize different vesicle generation pathways. It is found that RBCs can generate protein-rich soft vesicles, possibly driven by protein aggregation, and low membrane–protein content stiff vesicles, likely driven by cytoskeleton-induced buckling. Since similar cortical cytoskeleton to that of the RBC exists on the membranes of most mammalian cells, our findings help advancing the understanding of the fundamental process of vesicle generation.

1. Introduction

Extracellular vesicles (EVs), exosomes and microvesicles, are important mediators of cell–cell communication.^[1] By transferring signaling molecules, EVs play a key role in a wide range of physiological processes as well as spreading of diseases,^[2,3] including cancer metastasis.^[4] In order to generate vesicles, or to uptake them, membranes need to undergo dramatic deformations. Consequently, mechanical properties of membranes have a vital role in such processes.

Proteins occupy $\approx 20\%$ of the hydrophobic layer of the membrane of red blood cells (RBCs),^[5] as well as of the membrane of synaptic vesicles.^[6] The effect of bulky, transmembrane proteins on bending modulus of membranes has been considered in a limited number of studies. For bacteriorhodopsin, the bending modulus did not

Dr. R. Sorkin, F. Bošković, Dr. D. Vorselen, Prof. G. J. L. Wuite
Department of Physics and Astronomy and LaserLab
Vrije Universiteit Amsterdam
Amsterdam, 1081 HV, the Netherlands
E-mail: sorkin.raya@gmail.com, r.s.sorkin@vu.nl; gwuite@nat.vu.nl

Dr. R. Huisjes, S. Pignatelli, Prof. R. M. Schiffelers
Department of Clinical Chemistry and Haematology
University Medical Center Utrecht
Utrecht, 3584 CX, the Netherlands


Dr. Y. Ofir-Birin, Dr. N. Regev-Rudzki
Department of Biomolecular Sciences
Weizmann Institute of Science
Rehovot 761000, Israel

J. K. Freitas Leal, Dr. G. Bosman
Department of Biochemistry
Radboud University Medical Center
Radboud Institute for Molecular Life Sciences
Nijmegen, NL-6500 HB, the Netherlands

Dr. J. Schiller
Institute of Medical Physics and Biophysics
University of Leipzig
Medical Faculty
Härtelstr. 16/18, 04107, Leipzig, Germany

D. Mullick
Department of Chemical and Biological Physics
Weizmann Institute of Science
Rehovot 761000, Israel

Prof. W. H. Roos
Department of Molecular Biophysics
Zernike Instituut
Rijksuniversiteit Groningen
Nijenborgh 4, Groningen, 9747 AG, the Netherlands

 The ORCID identification number(s) for the author(s) of this article can be found under <https://doi.org/10.1002/smll.201801650>.

DOI: 10.1002/smll.201801650

show any measurable dependence on protein concentration in the vesicles,^[7] but a significant reduction in bending modulus values was observed when Ca-ATPase was added to giant unilamellar vesicles.^[8] Moreover, recent simulations have shown that integral membrane proteins can have diverse effects on membrane mechanics, either softening, neutral, or stiffening.^[9] None of these studies, however, have considered the effect of a large variety of proteins on the mechanics of membranes of complex lipid mixtures.

While membrane mechanics likely plays a role in vesicle budding, unlike exosome biogenesis, microvesicle generation is not well understood. Vesiculation driven by aggregation of membrane proteins of mutual affinity is one possibility,^[10] probably involving formation of membrane microdomains and rearrangement of membrane phospholipids driven by enzymes such as translocases and scramblases.^[11] Moreover, cytoskeleton compression-induced membrane-buckling can result vesicle budding.^[10,12,13] Cytoskeletal elements and their regulators are known to be required for vesicle biogenesis in several cell types: actin dynamics regulators from the RHO family of small GTPases were demonstrated to induce microvesicle biogenesis in different populations of tumor cells,^[14] while myosin-1a excreted forces lead to formation and release of gut microvesicles.^[15] Despite this available information, the relative importance of these process in vesicle generation, namely protein aggregation versus cytoskeletal forces, is hard to elucidate.

Here we use nanomechanics as a quantitative tool^[16,17] to study vesicle generation and natural membrane mechanics. We use mainly RBC-derived vesicles that are a good model system, because RBCs lack intracellular organelles and thus the generated EVs are exclusively derived from the cell membrane. Moreover, RBC-derived EVs are also biologically important as coagulation promoters that may also have immunosuppressive activities,^[18] as well as mediators of communication between *Plasmodium falciparum* (Pf)-infected RBCs during malaria infection.^[19,20] With the aim to understand mechanics of natural vesicles, and their generation pathways, we study vesicles from healthy and malaria infected RBC, as well as vesicles from a fibrosarcoma cell line, in addition to RBC under different temperature treatments. We hypothesize that by keeping RBC at different conditions different vesiculation mechanisms may be triggered, as a result of, e.g., slowing down of enzymatic processes at low temperatures, possibly leading to vesicles of different mechanical properties. We find that indeed, depending on incubation temperature, RBC can generate protein-rich soft vesicles, possibly driven by protein aggregation, and low membrane–protein content stiff vesicles, likely driven by cytoskeleton induced buckling. Overall, our results shed new light on the poorly understood process of EV release by plasma membrane budding.

2. Results

2.1. Vesicles from Various Cell Types Are Mechanically Similar

In order to understand the extent of variation in mechanics of natural vesicles, we examined three very different vesicle populations: EVs formed by RBCs from a healthy donor, EVs generated by Pf-infected RBCs, which are a mixture of vesicles originating

in the RBC membrane as well as parasite-derived EVs,^[19] and vesicles from a fibrosarcoma-derived cell line (HT1080 cells). We expected mechanical differences in these vesicle populations for the following reasons: first, healthy RBC vesicles are different from vesicles secreted by Pf-infected RBCs in size, protein composition, and the number of EVs generated per cell^[19] (size distributions measured by nanoparticle tracking analysis (NTA) are shown in Figure S1, Supporting Information). Second, the exosome-like vesicles originating from the parasite-infected cells have a role in cell–cell communication, as described in the introduction. We therefore hypothesized that these EVs might be mechanically optimized for uptake by their target cells. Further, a cancer cell line was chosen as it is known that cancer exosomes are involved in cancer metastasis.^[4] Isolated EVs from HT1080 cells, in fact, consist of a mixture of membrane shed microvesicles and exosomes, which is typical for many cell types. In the case that these populations are mechanically different, we would expect to see two subpopulations in our analysis. Prior to isolation of EVs, healthy RBCs, Pf-infected RBCs and HT1080 cells were all incubated for 20 h at 37 °C.

We have recently developed a quantitative model based on Canham-Helfrich^[21,22] theory that showed that the mechanical properties of adherent nanovesicles can be understood in terms of membrane bending and internal osmotic pressure. Using this methodology, the bending modulus of small (30–200 nm) synthetic vesicles,^[17] as well as natural vesicles from RBCs^[16] can be assessed using the experimentally obtained values for vesicle stiffness, radius, and tether force.^[17] We have applied this approach to the EVs detailed above as follows: first, with high-resolution imaging we determined the shape of the EVs and revealed that they maintain a rounded shape (Figure 1A). These images are then used to accurately extract vesicle radius of curvature, R_c . To do this correctly, we applied a correction for the tip shape and a correction for deformation due to applied imaging forces (see Experimental Section and ref. [17]). Subsequently, we quantified the shape of EVs by measuring the height over the radius of curvature. From this data, we calculated the unperturbed radius of the vesicles (Figure S1B, Supporting Information), assuming surface area conservation.^[17] Figure S1 (Supporting Information) shows that the size distributions of vesicles as determined by atomic force microscopy (AFM) imaging are generally similar to those obtained from NTA. We have previously demonstrated that our approach is applicable for vesicles within this size range.^[17] Second, force indentation curves (FDCs) were recorded; the curves were obtained by moving the tip to the center of the EV and indenting it until a preset force is reached (schematic drawing in Figure 1B). Before each vesicle indentation, the tip was always first pushed against a bare surface, to validate its cleanliness manifested as a typical glass curve (without hysteresis and indentation). Typically, first a force of 500 pN was applied on the center of the EV, followed by a subsequent indentation until a force of 10 nN is reached. These plots overlap, as can be seen in the black and red curves in Figure 1C–E, implying elastic behavior at this initial indentation stage. An initially linear response is followed by a superlinear response, then followed by, in ≈40% of the cases, a shoulder corresponding to inward tether formation, and then a sharp increase in stiffness, followed by a discontinuity, most likely corresponding to lipid bilayer penetration.

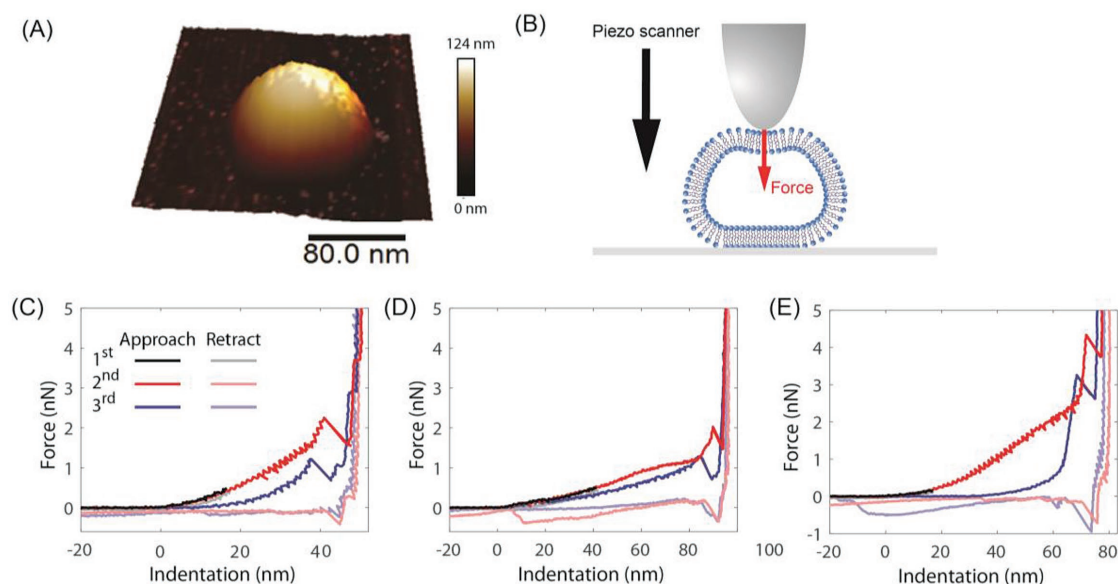


Figure 1. AFM imaging and nanoindentations of EVs. Isolated EVs, dispersed in PBS, were attached to poly-L-lysine coated surfaces. A) An image of a typical vesicle isolated from Pf-infected RBC. B) Schematic illustration of the nanoindentation experiment: the tip indents the vesicle until a preset force is reached. Typical force plots for C) vesicles from healthy RBC, D) vesicles from Pf-infected RBC, and E) vesicles from fibrosarcoma cell line, HT1080 cells.

(Figure 1C–E). Such behavior is characteristic for fluid nanovesicles.^[17] Images of vesicles before and after indentation are shown in Figure S2 (Supporting Information).

The stiffness of EVs was found by fitting the linear response for indentations up to $0.1 R_c$. To estimate the osmotic pressure over the membrane, which results from water loss during vesicle adsorption to the surface, the retrace of indentation curves was analyzed. A tether, marked by a force plateau with force F_t , was detected during the retrace in $\approx 56\%$ of FDCs for healthy RBC vesicles at 37°C . The tether force equals $F_t = 2\pi\sqrt{2\sigma\kappa}$, with σ the tension in the membrane and κ the

bending modulus of the membrane.^[23] We then estimate the tension in the membrane using the Young-Laplace equation: $\Delta\Pi = 2\sigma/R_c$, with $\Delta\Pi$ being the osmotic pressure difference over the membrane. With these measurements of the radius of curvature, the stiffness and the tether force, we used our recent model to fit the bending modulus of the vesicles.^[17] Importantly, this allows us to compare various vesicle populations, as a bending modulus is an intrinsic material property of the vesicles and does not depend on, e.g., vesicle size.

In Figure 2A, fitting of the experimental data to the theoretical normalized stiffness versus normalized pressure curve for

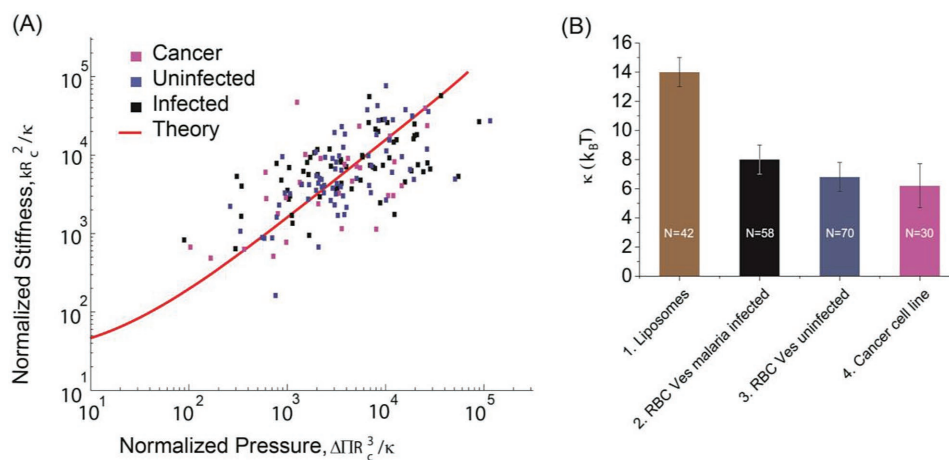


Figure 2. Bending modulus estimation for EVs of different origins, isolated after 20 h incubations at 37°C . A) Dimensionless pressure versus dimensionless stiffness for EVs from pf-infected RBCs, healthy RBCs, and fibrosarcoma cell line, HT1080 cells. Red line is the theoretically predicted curve. Different colored symbols are the experimental data for three vesicle types, as indicated in the inset. Same colors are used in (B). Bending modulus was used as single fitting parameter, separately for each of the vesicle types. B) Bending modulus estimates for the three vesicle populations and liposomes. Error bars mark 68% confidence intervals determined by bootstrapping. Liposome bending modulus value adapted Vorselen et al.^[17] for 200 nm extruded vesicles with lipid composition mimicking the RBC lipid membrane.

the three different vesicle populations is shown. The bending modulus was individually fit for each one of the three populations. The resulting values of κ obtained from each of the fits are given in Figure 2B. It can be clearly seen that the κ values are very similar for the three vesicle populations; $\kappa = 8 \pm 1$ for vesicles from Pf-infected RBCs, $\kappa = 7 \pm 1$ for vesicles from healthy RBCs and $\kappa = 6 \pm 2$ for vesicles from HT1080 cells. Surprisingly, these vesicles that are of different cellular origin are nonetheless mechanically similar. Possibly the mechanical properties of vesicles are rather universal across cells from different origins. The bending modulus of pure lipid liposomes, with a composition that mimics the lipid composition of a RBC membrane, is shown for comparison. (Data adapted from Vorselen et al.^[17]).

The results of bending moduli obtained by this analysis are very robust, and donor independent for the RBC. Moreover, the results were independent of the isolation protocol, independent of which lab was performing the isolation procedure, and unaffected by freezing and thawing of the supernatant, as well as similar for different healthy donors. A detailed account of these analyses is provided in the supplementary data and Figure S3 (Supporting Information).

2.2. Vesicles Isolated from Fresh RBCs are Softer

Following the surprising discovery that vesicles isolated from different cells, all obtained by incubation of the cells for 20 h at 37 °C prior to EV extraction, are mechanically similar, we aimed to explore the triggers that might modify vesicle mechanics by examining the effect of cell incubation time and temperature on the bending modulus of healthy donor RBC vesicles. To test the effect of RBC sample freshness on vesicle mechanics, we have isolated RBCs immediately after blood drawing, and then incubated the RBC in Ringer buffer for 2 h. After 2 h, vesicles were directly isolated by either size exclusion chromatography (SEC) or differential centrifugation. The resulting vesicles showed a mean value of $\kappa = 3 k_B T$ (Figure 3A). To examine the effect of RBC incubation time on vesicle mechanics, we further examined the vesicles obtained from fresh RBCs stored for 20 h in Ringer buffer and from RBCs stored in blood bank conditions for 35 d. For all three different incubation times, vesicles were isolated from RBC kept at 4 °C for the indicated time period, and then directly isolated, so that effectively vesicles secreted from $t = 0$ until the indicated time point were present in the

sample. We found that vesicles isolated from RBCs after 2 h of incubation are significantly softer than after longer incubation times, whereas they do not vary significantly between 20 h and 35 days (Figure 3A). Further, we find that there is a large difference in the size of vesicles: after 2 h, $R_0 = 35 \pm 1$ nm, after 20 h, $R_0 = 85 \pm 3.5$ nm and after 35 d: $R_0 = 59 \pm 3$ nm (Figure 3B), with R_0 the original vesicle radius before adhesion assuming surface area conservation.^[17] This suggests that different vesicle generation mechanisms previously suggested theoretically,^[10] dominate at different incubation times.

2.3. Temperature during RBC Incubation Affects Vesicle Mechanics

We hypothesized that by keeping RBC at different conditions, different vesiculation mechanisms may be triggered, as a result of, e.g., slowing down of enzymatic processes at low temperatures- possibly leading to vesicles of different mechanical properties. We find that temperature during RBC incubation indeed affects the bending modulus of the generated vesicles, in a surprising nonlinear fashion: the lowest value of $5 \pm 0.8 k_B T$ is found for 4 °C, whereas the highest bending modulus value of $13 \pm 1 k_B T$ is obtained for RT (22 °C) and a value of $6.8 \pm 1 k_B T$ for the 37 °C (Figure 4). To better understand the origins of these differences in mechanics of the three vesicle populations due to the different temperature conditions, we performed lipid analysis of these vesicles. The results of our lipidomics analysis are shown in Figure S2 (Supporting Information). We have used MALDI-TOF (matrix-assisted laser desorption and ionization) MS (mass spectrometry)^[24] to screen the compositions of the lipid extracts from erythrocyte ghosts (as the control) and different vesicles at different temperatures (Figure S2, Supporting Information).

When comparing the vesicles spectra to the ghosts spectra, one striking difference is the presence of lysophosphatidylcholine (LPC) 16:0 (m/z 496.3 and 518.3) and LPC 18:0 (m/z 524.3 and 546.3) in the vesicles, but not in the RBC membranes (Figure S4, Supporting Information). A significantly higher concentration of LPC has been described before for platelet-derived microparticles, suggesting that this may be a general phenomenon.^[25] Formation of LPC indicates that there is either an activation of phospholipases or an increased generation of reactive oxygen species, which are also able to convert phospholipids into the corresponding lysolipids. The activation of phospholipase A₂ (PLA₂) seems

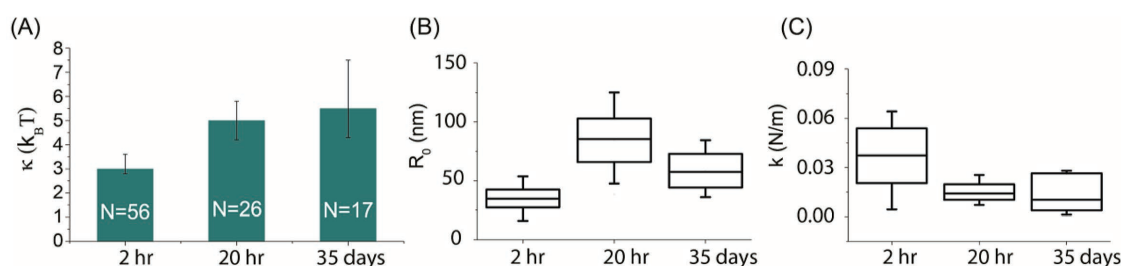


Figure 3. Bending modulus A) size B) and stiffness C) of vesicles from different incubation times of RBCs at 4 °C. Vesicles obtained after 2 h at 37 °C were very similar to vesicles obtained after 2 h at 4 °C. (Not shown, unperturbed radius of 48 ± 3.5 nm SEM, $N = 34$, $\kappa = 3.5 \pm 0.5 k_B T$ 68% confidence intervals determined by bootstrapping).

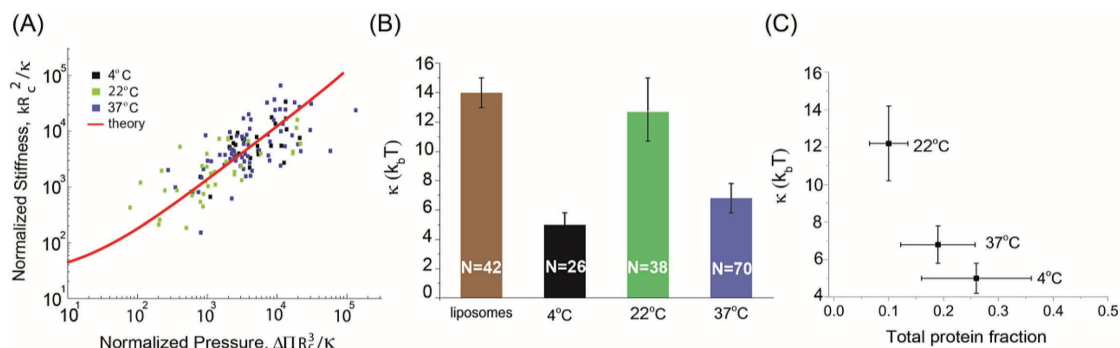


Figure 4. Effect of temperature during RBC incubation on bending modulus of the secreted vesicles. A) Dimensionless pressure versus dimensionless stiffness for EVs from RBCs from healthy donors at different incubation temperatures of RBC during vesicle secretion. Red line is the theoretically predicted curve. Different colored symbols are the experimental data for three vesicle types, as indicated in the inset. Bending modulus was used as single fitting parameter. B) Bending modulus values of the three vesicle populations and synthetic liposomes (synthetic liposome value from Vorselen et al.^[17] for 200 nm extruded vesicles with lipid composition mimicking the RBC lipid membrane), showing significantly different moduli at different temperatures, which are either comparable to or lower from the bending modulus of pure lipid liposomes. Error bars mark 68% confidence intervals determined by bootstrapping. C) The bending modulus values at different temperatures plotted as a function of the calculated protein fraction values.

the most reasonable explanation of the observed effects: this enzyme converts PC into lysophosphatidylcholine (LPC) but does not digest SM. Formation of LPC may be involved in the vesiculation process, as lysolipids have been previously demonstrated to be facilitators of budding and fission in synthetic systems,^[26,27] likely due to their inverted cone shape, which stabilizes positively curved structures. Moreover, LPC could have an additional indirect effect by affecting Ca^{2+} homeostasis.^[28] Yet, neither the presence of LPC nor the observed lipid composition does not help explain the mechanical differences we observe due to temperature.

What we did notice however is that all natural vesicles were softer than pure lipid liposomes, or mechanically similar, as can be seen in Figure 4B. Hence, the presence of membrane proteins seems to be important in the lowering of the bending modulus and the amount of membrane protein might be the determining factor for the decrease. In order to estimate the amounts of protein present, we further quantified the total phospholipid content of vesicles generated at different temperatures, as shown in Figure 4C and described in detail in the supplementary data and Figure S4 (Supporting Information). We chose to quantify the lipids rather than the proteins, as lipids are only found in the membrane, while proteins can be found both as cargo within the vesicles as well as plasma-derived proteins attached to the vesicle exterior. Therefore, a clean isolation of the integral membrane proteins is not straightforward. Since contamination of the vesicle lipid component by plasma lipids is much less likely to occur,^[29] indirect quantification of the protein content from the lipid analysis is a more reliable approach. We calculated the estimated total area fraction of proteins in the membrane of the different natural vesicles, assuming phospholipid fraction + cholesterol fraction + protein fraction = 1. This calculation is a rough estimation, due to the use of an average vesicle diameter and an average lipid head-group area values. Nonetheless, we do observe a trend of reduction in the bending modulus values as the total phospholipid amount decreases, which likely correlates with an increase in the total protein fraction/vesicle.

3. Discussion

In this study, an in-depth examination of a broad range of EVs is undertaken, providing insights to the largely unexplored field of mechanics of natural vesicles. Very few previous pioneering studies addressed the importance of mechanical properties of extracellular vesicles^[30,31] and so far the pressurization of vesicles due to surface interactions has not been taken into account. Our recently developed approach^[16,17] does take pressurization into account. It allows reliable comparison of different vesicle populations, as we are able to estimate the bending modulus of the vesicles, an intrinsic material property that is independent of the measuring conditions. One striking observation in our study is the similarity in the mechanics of vesicles from different cells and origins, as well as isolation methods, blood donors, and experimentalists performing the vesicle isolation. We find that bending modulus values obtained here for RT incubated RBC are very comparable to those we previously measured in a different set of experiments with vesicles produced at similar conditions of RT 20 h incubation,^[16] demonstrating again the robustness of our method.

Vesiculation may generally occur by a protein-aggregation driven mechanism, or by cytoskeletal compression-induced buckling^[10,32] (Figure 5). It is possible that both mechanisms coexist, while the balance between them is shifted in different conditions. Presumably, different pathways will lead to different mechanical properties. We therefore test the effect of temperature on the mechanical properties of the generated EVs. We indeed find that RBCs generate vesicles of different mechanical properties at different incubation temperatures (Figure 4). Could changes in the lipid composition, or the protein composition, explain these differences? When considering the extent of variation in the lipid composition of vesicles generated at different conditions, this variation is not larger than the variation between different donors (Figure S2, Supporting Information). Similarly, a variation in the protein composition of vesicles from different donors has been previously reported for EVs,^[33] as well as for RBC-derived vesicles in particular.^[34] Despite this variability, we

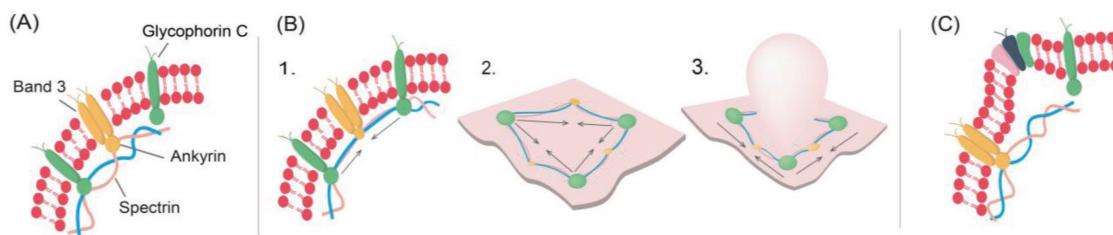


Figure 5. Vesicle generation at the RBC membrane. A) At normal ATP levels, actin-band 4.1 complex interacts reversibly with glycoprotein C, resulting in binding and unbinding at the ends of spectrin filaments. B) At low ATP levels, no unbinding occurs, thus leading to increased cytoskeletal compression, as illustrated by the arrows in (B) 1 and 2. This compression, upon reaching a critical value, results buckling of the bilayer within the cytoskeleton unit, as illustrated in (B) 3. C) Another mechanism contributing to vesicle generation—the aggregation of proteins that modify membrane curvature. Illustration by Katia Morozkin, based on work by N. Gov and others.^[10,37]

find that the bending modulus is in fact a very robust and reproducible property of the vesicles and not dependent on the specific lipid and protein profiles. This suggests that the differences in bending modulus between vesicles produced at different temperatures cannot be explained by a change in the amount of a certain lipid or protein component, or the introduction of a new lipid/protein. What seems more reasonable, instead, is that the ratio of total amount of proteins to the total amount of lipids is dominating the mechanical behavior. To test this hypothesis, we analyzed the total number of lipids and estimated the protein/lipid ratio (Figure 4C), as explained in detail in the Supporting Information. The obtained values ($\approx 20\%$ proteins in the membrane of 37°C vesicles) are in line with previously reported values for the protein content of natural membranes.^[5] Our analysis of the total phospholipid content of vesicles generated at different temperatures indeed suggests that vesicle bending modulus decreases with increased protein content.

We suggest the following explanation for the observed mechanical differences between the different EVs, and their relation to vesiculation mechanisms. Generation of stiffer vesicles at 22°C compared with 37°C is probably related to lower ATP levels at 22°C . Several studies demonstrated that ATP-driven cytoskeleton forces lead to membrane softening in RBCs^[35–38] as consumption of ATP promotes spectrin–actin dissociation due to phosphorylation of protein-4.1.^[39–41] Lower ATP concentrations correspond to a denser cytoskeleton, and hence higher contractile forces that are exerted on the membrane (see Figure 5B). Such higher contracting forces could enable buckling also in less soft areas of the membrane that have lower protein content, which will normally not vesiculate, leading to the generation of vesicles that have a higher bending modulus. At these conditions, cytoskeletal induced buckling is probably more dominant than protein-aggregation mediated vesiculation. The similarity in bending modulus values of vesicles generated by different cell types, healthy RBC, malaria infected RBC, and a fibrosarcoma cell line, all at 37°C , suggests that at physiological temperatures, membrane composition is dominating vesicle formation (see Figure 5C). At these conditions, budding possibly occurs preferentially at areas of the membrane that have a certain protein/lipid ratio that results a low enough bending modulus, such that the energy barrier for budding can be overcome more easily. This explanation is also in line with our result of low bending modulus at short incubation times; at short incubation times, vesiculation first occurs at preferential, softer spots of the membrane,

possibly those containing more protein. Finally, lower bending modulus of RBC EVs generated at 4°C compared with 22°C might be due to insufficient thermal energy, as the flow of the membrane into the forming bud is slowed down at this cool temperature. Therefore the regions that bud most quickly are the only ones that are observed, and these are biased towards the softest, protein-rich regions in the membrane. Our findings therefore support the idea^[10] that several different budding mechanisms may be involved in generation of membrane shed vesicles. Since similar cortical cytoskeleton to that of the RBC exists on the membranes of most mammalian cells and on the membranes of internal organelles^[42] our findings help advancing the understanding of the fundamental process of vesicle generation.

4. Experimental Section

Cell Cultures/Incubations: HT1080 cells (fibrosarcoma cell line) were cultured in DMEM medium supplemented with 10% exosome-free FBS (Thermo Fisher Scientific). *P. falciparum* asexual stage parasites were maintained in culture in human O^+ erythrocytes at 4% hematocrit in RPMI-HEPES supplemented with Albumax (0.5% w/v, Invitrogen) as previously described.^[19]

EV Isolation: Vesicles were isolated by one of two methods, differential centrifugation or size-exclusion chromatography (SEC), as indicated in the text for each vesicle preparation. For vesicles from healthy RBC, both protocols were compared and the vesicles were found to have similar bending modulus values (see results section). EV isolation from Pf-iRBCs was performed as previously described.^[19]

EV Isolation by SEC: 50 mL of cell culture supernatant was concentrated to $\approx 500\ \mu\text{L}$ by Amicon Ultra-15 centrifugal filter units, and then loaded on qEV SEC columns.^[43] The eighth and ninth fractions were collected and then used for further analysis.

Red Blood Cell EVs Isolation by Differential Centrifugation: Blood from healthy donors was collected in heparin tubes. Whole blood was centrifuged ($1000 \times g$, 10 min) and washed three times with HEPES-buffered Ringer solution ($10 \times 10^{-3}\ \text{M}$ HEPES, $5 \times 10^{-3}\ \text{M}$ KCl, $2 \times 10^{-3}\ \text{M}$ CaCl_2 , $120 \times 10^{-3}\ \text{M}$ NaCl, $0.8 \times 10^{-3}\ \text{M}$ MgCl_2 , pH 7.4). After each centrifugation step, the buffy coat and top RBC part were aspirated and discarded. During incubation RBCs were resuspended in HEPES-buffered Ringer solution (pH 7.4) with $5 \times 10^{-3}\ \text{M}$ glucose to yield a final hematocrit of 40%. RBCs were incubated for 20–22 h, while tumbling. This was done at 37°C , except for experiments specifically aimed at looking into the effect of temperature on vesicle mechanics, as described in the text. RBCs were centrifuged for 10 min at $1000\ g$. Supernatant was diluted 10 times in HEPES-buffered Ringer solution and centrifuged again to remove residual RBCs. Big particles were depleted by centrifugation for 10 min at $10\ 000\ g$. Supernatant of $10\ 000\ g$ pellet was spun for 70 min

at 100 000 g to pellet EVs. EVs were washed once in HEPES-buffered Ringer solution. All EV isolation steps were performed at 4 °C.

For the study of the effect of incubation time on vesicle mechanics, two samples from cells at 37 °C were prepared by two different labs (Utrecht and Nijmegen). Vesicles were isolated by SEC by the Nijmegen lab and by differential ultracentrifugation by the Utrecht lab.

Ghost Membrane Preparation: Washed RBCs were diluted in hypotonic phosphate buffer (1.4×10^{-3} M NaH_2PO_4 , 5.7×10^{-3} M Na_2HPO_4) supplemented with cOMplete protease inhibitor cocktail (Roche) and were incubated for 2 h at 4 °C while gently tumbling. Ghost membranes were spun down at 43 000 x g for 10 min, without brake. Membranes were washed till pellet was transparent and free of hemoglobin. Ghost membranes were resuspended in HEPES buffered saline (HBS, 10×10^{-3} M HEPES, 150×10^{-3} M NaCl, pH 7.4).

AFM Experiments: EVs were adhered to poly-L-lysine coated glass slides in PBS. Slides were cleaned in a 96% ethanol, 3% HCl solution for 10 min. Next, they were coated for 1 h in poly-L-lysine (a 0.001% Sigma) solution, rinsed with ultrapure water, and dried 20 h at 37 °C. They were stored at 7 °C for maximally one month. A 10 μL drop of vesicle dispersion in PBS was incubated on the glass slide. Vesicles were imaged in PeakForce Tapping mode on a Bruker Bioscope catalyst setup. Imaging was always done at RT, about 22 °C. Force set point during imaging was 100–200 pN. Nanoindentations were performed by first making an image of a single particle, then indenting it until a trigger force of 0.5 nN is reached, and subsequently applying higher forces (2–10 nN) at a velocity of 250 nm s^{-1} . After indentation, typically another image was recorded to check for movement or collapse of the vesicle. Importantly, both before and after the vesicle indentation, the tip was checked for adherent lipid bilayers by recording a force–distance plot on the glass surface until a trigger-force of 5 nN. Tips used were either silicon nitride tips with a nominal tip radius of 15 nm on a 0.1 N m^{-1} cantilever by Olympus (OMCL-RC800PSA) or Bruker SNL silicon nitride tips on a 0.12 N m^{-1} cantilever with a nominal tip radius of 2 nm. Individual cantilevers were calibrated using thermal tuning.

AFM Image Analysis: Both images and force curves were processed using home-built MATLAB software. Size and shape were analyzed from line profiles through the maximum of the vesicle along the slow scanning axis. Circular arcs were fit to the part of the vesicle above half of the maximum height to obtain the radius of curvature, from which the tip radius (2 nm/ 15 nm, as provided by the manufacturer) was subtracted. The height of vesicles was derived from FDCs, and the difference between the height obtained from FDCs and images was used for a subsequent correction of R_c .^[17] R_0 , the unperturbed vesicle radius in dispersion, was calculated under the assumption of surface area conservation as previously described.^[17]

AFM FDC Analysis: Analysis was done as described in detail previously. Briefly, raw data of a force cycle, given by the deflection of the cantilever versus the Z-piezo displacement, was converted to force versus separation (between the tip and the sample, or FDC) by subtracting the cantilever deflection. Contact point between tip and vesicle was found by using a change point algorithm and occasionally manually adjusted. Before fitting, FDCs (10 k data points) were smoothed (moving average with window length of ≈ 10 points). Stiffness of the EVs was found by fitting a straight line in the interval between 0.02 and 0.1 R_c . For finding the tether force, a step fitting algorithm based on the change point algorithm was used, which divides the curve into segments with slope 0. Only adhesion events extending beyond the contact point were included. For fitting to the theory, described in detail elsewhere,^[17] the sum of the squared log Euclidian distance between the theoretical curve and the individual experimental data points was then minimized by adjusting κ as a single fitting parameter. Confidence intervals were estimated using the bias corrected percentile method with 1000 bootstrapping repetitions, for which a set of observed value combinations equal in size to the original data set was randomly drawn and fitted.

Nanoparticle Tracking Analysis: EVs were sized by recording 5 videos of 60 s using the NanoSight LM10 system (Malvern Instruments). A camera level of 14 was used and videos were recorded at 22 °C. Analysis

of the videos was performed using the NTA 2.0 software, using default settings. Threshold was set at 5.

Supporting Information

Supporting Information is available from the Wiley Online Library or from the author.

Acknowledgements

The authors are grateful to Nir Gov for numerous illuminating discussions. The authors thank Edwin van der Pol, Rienk Nieuwland, Rubina Baglio, and Michiel Pegtel for useful discussions and for generously allowing us to use their equipment. The authors thank Fred MacKintosh for useful discussions. R.S. acknowledges support through HFSP postdoctoral fellowship LT000419/2015, as well as support through the Israeli National Postdoctoral Award for Advancing Women in Science, and the L'Oreal UNESCO award for advancing women in science. J.K.F.L. acknowledges the support by the National Council for Scientific and Technological Development—Brazil. W.H.R. acknowledges support by the Nederlandse Organisatie voor Wetenschappelijk Onderzoek (NWO) for a VIDI grant. The authors are grateful to the Electron Microscopy Unit at the Weizmann Institute of Science for their assistance with cryo-EM imaging of EVs.

Conflict of Interest

The authors declare no conflict of interest.

Keywords

AFM, extracellular vesicles, membrane biophysics, RBC

Received: May 1, 2018

Revised: July 18, 2018

Published online:

- [1] N. Kastelowitz, H. Yin, *ChemBioChem* **2014**, *15*, 923.
- [2] S. EL Andaloussi, I. Maeger, X. O. Breakefield, M. J. A. Wood, *Nat. Rev. Drug Discovery* **2013**, *12*, 347.
- [3] N. S. Barteneva, E. Fasler-Kan, M. Bernimoulin, J. N. H. Stern, E. D. Ponomarev, L. Duckett, I. A. Vorobjev, *BMC Cell Biol.* **2013**, *14*, 23.
- [4] A. Becker, B. K. Thakur, J. M. Weiss, H. S. Kim, H. Peinado, D. Lyden, *Cancer Cell* **2016**, *30*, 836.
- [5] A. D. Dupuy, D. M. Engelman, *Proc. Natl. Acad. Sci. USA* **2008**, *105*, 2848.
- [6] S. Takamori, M. Holt, K. Stenius, E. A. Lemke, M. Gronborg, D. Riedel, H. Urlaub, S. Schenck, B. Brugger, P. Ringler, S. A. Muller, B. Rammner, F. Gräter, J. S. Hub, B. L. De Groot, G. Mieskes, Y. Moriyama, J. Klingauf, H. Grubmüller, J. Heuser, F. Wieland, R. Jahn, *Cell* **2006**, *127*, 831.
- [7] J. B. Manneville, P. Bassereau, D. Levy, J. Prost, *Phys. Rev. Lett.* **1999**, *82*, 4356.
- [8] P. Girard, J. Prost, P. Bassereau, *Phys. Rev. Lett.* **2005**, *94*, 088102.
- [9] P. W. Fowler, J. Helie, A. Duncan, M. Chavent, H. Koldso, M. S. P. Sansom, *Soft Matter* **2016**, *12*, 7792.

- [10] N. Gov, J. Cluitmans, P. Sens, G. J. C. G. M. Bosman, in *Advances in Planar Lipid Bilayers and Liposomes*, Vol. 10, Academic Press, Elsevier **2009**, pp. 95–119.
- [11] G. van Niel, G. D'Angelo, G. Raposo, *Nat. Rev. Mol. Cell Biol.* **2018**, 19, 213.
- [12] D. Allan, P. Thomas, A. R. Limbrick, *Biochem. J.* **1980**, 188, 881.
- [13] H. Kalra, G. P. C. Drummen, S. Mathivanan, *Int. J. Mol. Sci.* **2016**, 17, 170.
- [14] B. Li, M. A. Antonyak, J. Zhang, R. A. Cerione, *Oncogene* **2012**, 31, 4740.
- [15] R. E. McConnell, J. N. Higginbotham, D. A. Shifrin, D. L. Tabb, R. J. Coffey, M. J. Tyska, *J. Cell Biol.* **2009**, 185, 1285.
- [16] D. Vorselen, S. M. van Dommelen, R. Sorkin, R. van Wijk, R. M. Schiffelers, G. J. L. Wuite, W. H. Roos, *BioRxiv* **2017**, <https://doi.org/10.1101/212456>.
- [17] D. Vorselen, F. C. MacKintosh, W. H. Roos, G. J. L. Wuite, *ACS Nano* **2017**, 11, 2628.
- [18] A. Alaarg, R. M. Schiffelers, W. W. van Solinge, R. van Wijk, *Front. Physiol.* **2013**, 4, 365.
- [19] N. Regev-Rudzki, D. W. Wilson, T. G. Carvalho, X. Sisquella, B. M. Coleman, M. Rug, D. Bursac, F. Angrisano, M. Gee, A. F. Hill, J. Baum, A. F. Cowman, *Cell* **2013**, 153, 1120.
- [20] P. Y. Mantel, A. N. Hoang, I. Goldowitz, D. Potashnikova, B. Hamza, I. Vorobjev, I. Ghiran, M. Toner, D. Irimia, A. R. Ivanov, N. Barteneva, M. Marti, *Cell Host Microbe* **2013**, 13, 521.
- [21] P. B. Canham, *J. Theor. Biol.* **1970**, 26, 61.
- [22] W. Helfrich, *Z. Naturforsch. C* **1973**, 28, 693.
- [23] V. Heinrich, R. E. Waugh, *Ann. Biomed. Eng.* **1996**, 24, 595.
- [24] B. Fuchs, R. Suss, J. Schiller, *Prog. Lipid Res.* **2010**, 49, 450.
- [25] I. Losito, R. Patruno, E. Conte, T. R. I. Cataldi, F. M. Megli, F. Palmisano, *Anal. Chem.* **2013**, 85, 6405.
- [26] T. Nakano, I. Inoue, R. Shinozaki, M. Matsui, T. Akatsuka, S. Takahashi, K. Tanaka, M. Akita, M. Seo, S. Hokari, S. Katayama, T. Komoda, *Biochim. Biophys. Acta, Biomembr.* **2009**, 1788, 2222.
- [27] G. Staneva, M. Seigneuret, K. Koumanov, G. Trugnan, M. I. Angelova, *Chem. Phys. Lipids* **2005**, 136, 55.
- [28] J. H. S. Kabarowski, K. Zhu, L. Q. Le, O. N. Witte, Y. Xu, *Science* **2005**, 307, 206.
- [29] E. Lauren, F. Tigistu-Sahle, S. Valkonen, M. Westberg, A. Valkeajarvi, J. Eronen, P. Siljander, V. Pettila, R. Kakela, S. Laitinen, E. Kerkela, *Biochim. Biophys. Acta, Mol. Cell Biol. Lipids* **2018**, 1863, 1.
- [30] B. Whitehead, L. Wu, M. L. Hvam, H. Aslan, M. Dong, L. Dyrskjøt, M. S. Ostenfeld, S. M. Moghimi, K. A. Howard, *J. Extracell. Vesicles* **2015**, 4, 29685.
- [31] S. Sharma, H. I. Rasool, V. Palanisamy, C. Mathisen, M. Schmidt, D. T. Wong, J. K. Gimzewski, *ACS Nano* **2010**, 4, 1921.
- [32] P. Sens, N. Gov, *Phys. Rev. Lett.* **2007**, 98, 018102.
- [33] D.-K. Kim, B. Kang, O. Y. Kim, D.-S. Choi, J. Lee, S. R. Kim, G. Go, Y. J. Yoon, J. H. Kim, S. C. Jang, K.-S. Park, E.-J. Choi, K. P. Kim, D. M. Desiderio, Y.-K. Kim, J. Lötvall, D. Hwang, Y. S. Gho, *J. Extracell. Vesicles* **2013**, 2, 20384.
- [34] M. H. Antonelou, J. Seghatchian, *Transfus. Apheresis Sci.* **2016**, 55, 92.
- [35] T. Betz, M. Lenz, J. F. Joanny, C. Sykes, *Proc. Natl. Acad. Sci. USA* **2009**, 106, 15320.
- [36] N. S. Gov, S. A. Safran, *Biophys. J.* **2005**, 88, 1859.
- [37] Y. Park, C. A. Best, T. Auth, N. S. Gov, S. A. Safran, G. Popescu, S. Suresh, M. S. Feld, *Proc. Natl. Acad. Sci. USA* **2010**, 107, 1289.
- [38] R. Rodriguez-Garcia, I. Lopez-Montero, M. Mell, G. Egea, N. S. Gov, F. Monroy, *Biophys. J.* **2015**, 108, 2794.
- [39] V. Bennett, *Biochim. Biophys. Acta, Rev. Biomembr.* **1989**, 988, 107.
- [40] E. Ling, Y. N. Danilov, C. M. Cohen, *J. Biol. Chem.* **1988**, 263, 2209.
- [41] S. Manno, Y. Takakuwa, N. Mohandas, *J. Biol. Chem.* **2005**, 280, 7581.
- [42] N. S. Gov, *Phys. Rev. E* **2007**, 75, 011921.
- [43] A. N. Böing, E. van der Pol, A. E. Grootemaat, F. A. W. Coumans, A. Sturk, R. Nieuwland, *J. Extracell. Vesicles* **2014**, 3, 23430.